Hierarchical Clustering and Small Baseline Subset Differential Interferometric Synthetic Aperture Radar (SBAS-DInSAR) for Remotely Sensed Building Identification and Risk

remote sensing

MDPI

Article

Hierarchical Clustering and Small Baseline Subset Differential Interferometric Synthetic Aperture Radar (SBAS-DInSAR) for Remotely Sensed Building Identification and Risk Prioritisation

Yassir Hamzaoui [1], Marco Civera [1,*], Andrea Miano [2], Manuela Bonano [3], Francesco Fabbrocino [2], Andrea Prota [4] and Bernardino Chiaia [1]

[1] Department of Structural, Building and Geotechnical Engineering, Politecnico di Torino, Corso Duca degli Abruzzi, 24, 10129 Turin, Italy
[2] Department of Engineering, Telematic University Pegaso, Centro Direzionale ISOLA F2, 80143 Napoli, Italy
[3] Consiglio Nazionale delle Ricerche (CNR)—Institute for Electromagnetic Sensing of the Environment, Via Diocleziano 328, 80124 Naples, Italy
[4] Department of Structures for Engineering and Architecture, University of Naples "Federico II", Via Claudio 21, 80125 Naples, Italy
* Correspondence: marco.civera@polito.it

Abstract: The conventional Structural Health Monitoring (SHM) framework focuses on individual structures. However, preliminary studies are required at a large territorial scale to effectively identify the most vulnerable elements. This becomes particularly challenging in urban settings, where numerous buildings of varied shapes, ages, and structural conditions are closely spaced from one another. A twofold task is therefore required: the automated identification and differentiation of various structures, coupled with a ranking system based on perceived structural risk, here assumed to be linked to their deformation patterns. It integrates displacement measurements acquired through the Differential Synthetic Aperture Radar Interferometry (DInSAR) technique, specifically employing the full-resolution Small Baseline Subset (SBAS) approach coupled with Hierarchical Clustering. The effectiveness of this method is successfully demonstrated and validated in two selected areas of Rome, Italy, serving as case studies. The results of this vast-area scale monitoring can be used to select the constructions that need a more in-depth assessment.

Keywords: machine learning; Hierarchical Clustering; Differential Interferometric Synthetic Aperture Radar (DInSAR); Small Baseline Subset (SBAS); COSMO-SkyMed; QGIS; built environment

Academic Editor: Timo Balz

Received: 11 November 2024
Revised: 27 December 2024
Accepted: 29 December 2024
Published: 2 January 2025

Citation: Hamzaoui, Y.; Civera, M.; Miano, A.; Bonano, M.; Fabbrocino, F.; Prota, A.; Chiaia, B. Hierarchical Clustering and Small Baseline Subset Differential Interferometric Synthetic Aperture Radar (SBAS-DInSAR) for Remotely Sensed Building Identification and Risk Prioritisation. *Remote Sens.* **2025**, *17*, 128. https://doi.org/10.3390/rs17010128

1. Introduction

Satellite-based Structural Health Monitoring (SHM) is an area of research that has gained significant attention from structural engineers in the last few years. For example, satellite interferometry has been recently utilised to monitor slow-moving landslides impacting buildings [1], assess the structural integrity of bridges [2–5] and school buildings [6], and observe subsidence caused by tunnel excavation [7]. Nevertheless, despite these successful applications, various limitations still hinder the widespread adoption of satellite data; for instance, almost all studies are based on land subsidence analysis and not directly on the buildings themselves. Furthermore, the potentially damaging effects of subsidence are almost always only linked to one mechanism.

Following the processing of satellite data, the interpretation of structural behaviour is of fundamental importance, also in relation to the types of actions whose effects on

structures can be effectively monitored using interferometric techniques. In fact, it is evident that satellite data, the frequency of which depends on the satellite's passage over the area of interest and varies from a few days to a few weeks, provide good results in observing slowly evolving phenomena.

During their useful life, constructions interact first and foremost with the geological and environmental context in which they are built. Consequently, in addition to gravity loads and earthquakes, constructions are also subject to additional actions induced on the structure by environmental, meteorological, and subsurface instability phenomena, which are independent of the presence of the structure itself and which can generate displacements in the structure that can also be monitored using the interferometric technique. Therefore, to obtain an overall view of the actions that can determine movements that can be monitored by satellite interferometry, it is essential to know, on the one hand, the characteristics of the structure and, on the other hand, the geological context of the subsoil and the environmental context in which the construction itself is inserted.

Finally, it is evident that the interpretation phase of understanding structural behaviour through satellite data analysis is a complex activity since, if conducted incorrectly or even with reference to an unsuitable time horizon, it could lead to incorrect assessments of structural behaviour. Importantly, remote sensing measurements must be associated with individual buildings to provide specific and detailed information at the level of the single structure. This is not trivial in densely built areas like highly urbanised city centres.

Automating this task is crucial, as the current manual approach is excessively labour-intensive and time-consuming. This automatic identification process is essential for enabling further analyses, particularly the ranking of buildings based on their deformation history over recent years. Ultimately, this information can be used to identify the most at-risk structures.

This automated identification and preliminary ranking is, essentially, a machine learning problem, based on Knowledge Extraction from the provided dataset of satellite-borne interferometric measurement time histories.

This framework was first put forward in [8], where a DBSCAN-based method was proposed and validated. Then, in [9], the ADAfinder tool was applied to EGMS data for the Structural Health Monitoring of urban settlements.

Departing from these previous research works, here a Hierarchical Clustering (HC)-based alternative is proposed and benchmarked against the results of those previous works. The key conceptual and practical aspects are concisely discussed, relying on a real case study as a guided example of an actual implementation.

This work proposes using satellite data combined with machine learning tools to quickly assess the deformation condition of the entire urban headquarters by using satellite data as the sole input.

The clustering methodology is briefly introduced in Section 2. A description of the specific case studies follows in Section 3. A walkthrough application is then presented in Section 4, with all the intermediate steps and results for the automatic building identification for these two areas (both selected within the city of Rome, Italy, using the COSMO-SKY MED data presented in [10]). These results of the HC methodology include a direct comparison with the previously proposed (DBSCAN-based) approach as well. Then, two ranking methods and their application for selecting the buildings with the highest priority, based on different expected damaging mechanisms, are presented for the two case study areas in Section 5. The Conclusions end this paper.

2. Materials and Methods

In the following paragraphs, the Small Baseline Subset Differential Synthetic Aperture Radar Interferometry (SBAS-DInSAR) technique [11,12] and the Hierarchical Clustering algorithm are briefly recalled to keep this article concise. More details about the specific aspects can be found in the reference sources.

2.1. Overview of the SBAS-DInSAR Technique

In the last decades, new-generation radar systems with very high resolution (VHR) have been developed, particularly TerraSAR-X and COSMO-SkyMed, with a spatial resolution of a few square metres. At the same time, Structural Health Monitoring has seen significant advancements, with satellite-based techniques like DInSAR enriching monitoring capabilities. DInSAR can measure ground motion phenomena such as landslides, subsidence, earthquakes, or volcanic activity with millimetre-scale precision by processing a time series of SAR satellite acquisitions. This enables, for example, monitoring of the stability of slopes, mining areas, buildings, and infrastructure. The advantages of utilising such techniques lie in the possibility of remote monitoring without introducing on-site instrumentation. DInSAR is based on static monitoring and gives velocity maps and time series of displacements at territorial and local scales. Its non-intrusive nature allows for continuous monitoring without disrupting bridge operations, and it enables the exploration of historical data for trend analysis and proactive maintenance. SAR technology aboard orbiting satellites delivers high-resolution, weather-independent imagery of Earth's surface. DInSAR uses SAR technology to generate interferograms, which provide information on the phase differences between SAR images acquired at different times and from different orbital positions. These data can be used alone or in combination with other physically attached SHM instrumentations, if available.

The Small Baseline Subset (SBAS) methodology [11] is an established advanced DInSAR technique that can be used to obtain information on the temporal and spatial pattern of LOS-projected displacement components observed by radar, generating displacement time series and mean velocity maps with subcentimetre accuracy [10]. The SBAS approach is based on a large number of SAR images acquired in the studied area during a specific time interval and is based on the proper selection of interferometric SAR data pairs used to generate multiple temporal differential interferograms. Each of these represents the phase difference (depurated from the topographic contribution of the surface by exploiting a 1 arc second SRTM (30 m) Digital Elevation Model related to the investigated area) between two SAR images collected from the same location at different time steps [12,13]. Specifically, the selected pairs are characterised by a slight difference between the acquisition trajectories and a relatively short time interval between the related SAR, which allows mitigating noise effects, often referred to as decorrelation effects, that affect the generated interferograms and thus maximise the spatial density of DInSAR measurement points, which are known as Persistent Scatterers (PSs). Moreover, the selected DInSAR interferograms may be affected by additional, undesired phase patterns superimposed on the deformation signals due to possible orbital inaccuracies, which may impair the final quality of DInSAR ground displacement measurements. Such phase artifacts induced by possible orbital errors can be approximated with a linear (or quasi-linear) phase ramp in both azimuth and range directions, often referred to as "orbital ramps", which are easily estimated and compensated for in the SBAS processing [14]. Regarding the general accuracy of the full-resolution SBAS DInSAR products in the radar LOS, the resulting accuracy is on the order of 1–2 mm/y for what concerns the mean deformation velocity value and 5–10 mm on the single deformation measurement. These average accuracy values have been achieved by means of several

extensive comparative analyses between SBAS-DInSAR and in situ measurements (GPS, precision levelling, inclinometers. . .) in large areas on Earth [12,14,15].

To summarise, this satellite data-based technique [12] provides displacement and velocity measurements for Persistent Scatterers (PSs), which are reflective targets on the ground. The measurements pertain to the satellite's ascending (ASC) and descending (DES) acquisition geometries, which can be combined to determine the actual direction and value of each PS's displacement/mean velocity vector. As previously mentioned, PSs retrieved from the COSMO-SkyMed constellation were used in this analysis, focusing on the period from 2011 to 2019. Both ascending and descending orbits were utilised to maximise the spatial density of the information.

2.2. Hierarchical Clustering

Hierarchical Clustering (HC) belongs to the family of the so-called unsupervised learning algorithms. Among this group, HC is well-known for its ability to agglomerate data from the bottom up into a multilevel hierarchy. The implementation used here adheres to the standard definition (see [16], Algorithm 6.4.1) and involves three consecutive steps. First, the distance between every pair of objects in the dataset is calculated. Next, all objects are organised into a binary hierarchical cluster tree based on maximum proximity and a linkage function. Finally, the data are partitioned by "cutting" the complete hierarchical tree at a specified height determined by a user-defined threshold.

HC has been applied for many years for pole clustering in Automated Operational Modal Analysis—see, e.g., its uses in unsupervised dynamic identification, reported in [17,18]. In this specific application, instead, the 'objects' are the PSs, and the 'distance' is intended to be the Euclidean distance between them.

Three options were considered for the linkage function:

1. single (i.e., the shortest distance);
2. complete (farthest distance);
3. average (unweighted average distance) linkage.

Based on some preliminary tests, the single linkage function provided the best results and was therefore selected.

Similarly, after some preliminary tests, the minimum cluster distance was selected as the discriminant for the threshold setting. Its value was set according to the average distance between buildings in the areas of interest to return homogeneous clusters that actually represent the underlying buildings and their shapes.

2.3. Complete Flowchart of the Proposed Methodology

This section presents the methodology developed for defining and analysing at-risk buildings in urban areas through integrating satellite interferometric data and advanced machine learning techniques. The flowchart of the methodology, shown in Figure 1, illustrates the key steps of the process, which are divided into four fundamental phases:

- ➢ Acquisition and Processing of Satellite Data (red box): This step involves acquiring and processing SAR images for the area of interest over the relevant period (2011–2019). The images are processed using a multi-temporal DInSAR technique (specifically, the high-resolution SBAS-DInSAR algorithm) to obtain spatially dense maps of coherent measurement points, known as Persistent Scatterers (PSs).
- ➢ Clustering and Identification of Buildings (green box): In this phase, the Hierarchical Clustering algorithm is applied to the processed data, allowing the grouping of measurement points corresponding to each individual building in the area of interest. This process enables the automatic identification of buildings.

- Deformation Analysis of Buildings (yellow box): This step involves analysing the deformation evolution of each identified building over the observation period. The analysis focuses on the velocity trends and deformation characteristics for each building group, to identify those at higher risk of damage due to subsidence or instability.
- Priority Ranking (blue box): Based on the deformation analysis, buildings are ranked according to their relative risk levels. A distortion index is calculated for each building, allowing for the prioritisation of those requiring in situ monitoring or further investigation.

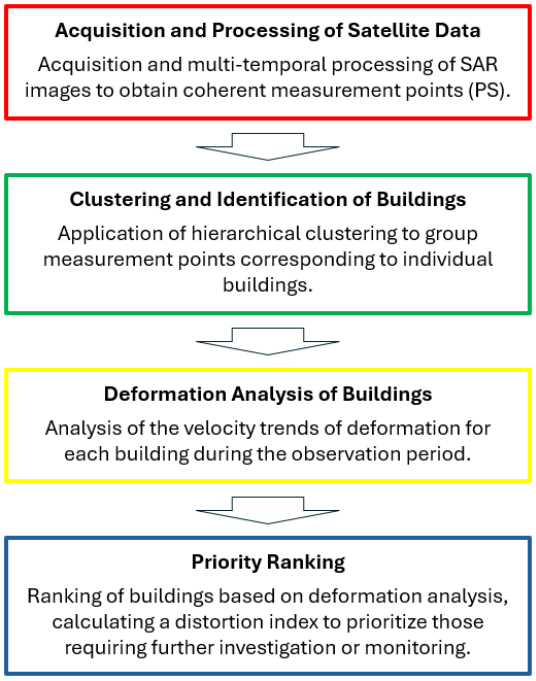

Figure 1. Flowchart of the proposed methodology.

The aspects related to the acquisition and processing of satellite data, as well as the Hierarchical Clustering identification process, are addressed in Sections 2.1 and 2.2. The remaining blocks of the procedure, focusing on deformation analysis and priority ranking, are described in greater detail in Section 5.

3. The Two Case Study Areas

The two areas of interest, named Area 1 (Figure 2a) and Area 2 (Figure 2b), are both included in the densely urbanised area. In particular, the case study areas are part of the city centre of the municipality of Rome (Italy), which has already been investigated in many previous studies on multi-temporal interferometric processing—see, e.g., [15,19–21]. In particular, the full-resolution SBAS-DInSAR approach [12] has been applied to two sets of SAR images collected from March 2011–March 2019 from ascending (ASC) and descending (DES) orbits, Stripmap mode (with a 3 m $\times$ 3 m ground resolution) by the sensors of the COSMO-SkyMed (CSK) constellation, and this evidenced some differential subsidence on the buildings in the selected areas [8].

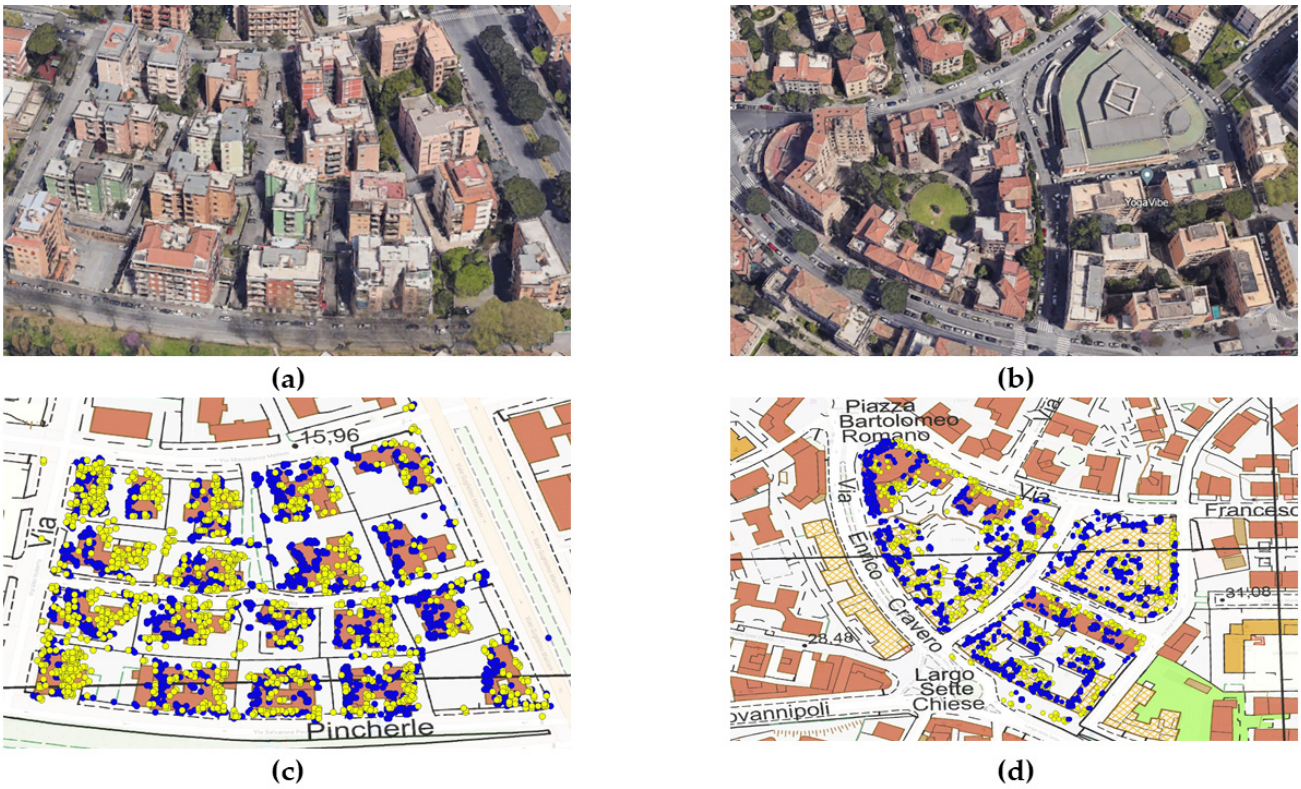

Figure 2. Top row: the two areas of interest: (**a**) Area 1 (circa 41°51′11″ N 12°28′17″ E) and (**b**) Area 2 (circa 41°51′42″ N 12°29′10″ E). Bottom row: the respective PS distributions. In (**c**,**d**), blue denotes ascending and yellow denotes descending orbits. Data retrieved from Google Earth (https://earth.google.com/web/, last accessed 23 December 2024) and COSMO-SkyMed (https://earth.esa.int/eogateway/missions/cosmo-skymed, last accessed 23 December 2024).

The available 129 ASC (frame HI-05) and 107 DESC (frame HI-03) CSK SLC images were paired to generate the overall sequences of interferometric SAR data pairs, consisting of a total of 392 ascending and 332 descending DInSAR interferograms, respectively. The differential interferograms were selected by imposing a maximum perpendicular baseline of about 1000 m and a maximum temporal baseline of 1800 days to limit the decorrelation effects and maximise the number of coherent pixels. Moreover, we used precise satellite orbital information and the 1 arcsec Shuttle Radar Topography Mission (SRTM) DEM of the study area (about 30 m of spatial resolution) to remove the topographic phase component from the DInSAR sequence. Finally, the generated DInSAR interferograms were unwrapped and subsequently inverted through the full-resolution SBAS-DInSAR approach [12], thus allowing us to retrieve the deformation time series (and the corresponding mean velocity measurements) for each PS.

More specifically, Area 1 and Area 2 include, respectively, 19 and 7 buildings. That is to say, Area 1 encompasses more structures, all of which are relatively well-separated and have simple shapes. In contrast, Area 2 contains fewer buildings, but they are larger and have more complex shapes. The building stock mainly consists of framed reinforced concrete structures. However, the choice was made just to cover different shapes and different heights without focusing on the representation of different structural typologies. Figure 2c,d also display the raw satellite data superimposed on the map obtained from the QGIS platform, an open-source software widely used for spatial data visualisation and analysis [22].

Importantly, as is discussed later, Area 1 was purposefully chosen to allow for direct comparability with the aforementioned DBSCAN-based technique, as this was the same application reported for validation in [8].

Conversely, Area 2 shows a completely different shape of the urban context; to this aim, the real potential of this procedure is to have reliable results in areas that present very different shapes between them (such as Area 1 and Area 2).

4. Building Identification and Shape-Finding Results

As mentioned at the beginning of this paper, the first aim of the proposed clustering technique was to automatically identify the data points corresponding to the same building. In turn, this enables automated and unsupervised building identification, including their number and—as especially relevant for Area 2—their actual shape in the plan view.

Thanks to the many reflective surfaces on the buildings, many PSs shown in Figure 2c,d correspond to actual structures. However, as a preliminary step, PSs referring to the ground surface between buildings must be removed. For this purpose, the information retrieved from the cumulative topographic distribution of the PSs can be exploited. In fact, for obvious reasons, building-related PSs will be localised at higher points. However, the difficulty lies in efficiently discriminating between these two groups in an unsupervised fashion. The maximum first derivative—indicating the maximum local difference—was chosen to automate this selection procedure to determine the cut-off height δ. As illustrated in Figure 3a,b, this corresponds to 34–36 m for Area 2 and slightly less (22–24 m) for Area 1.

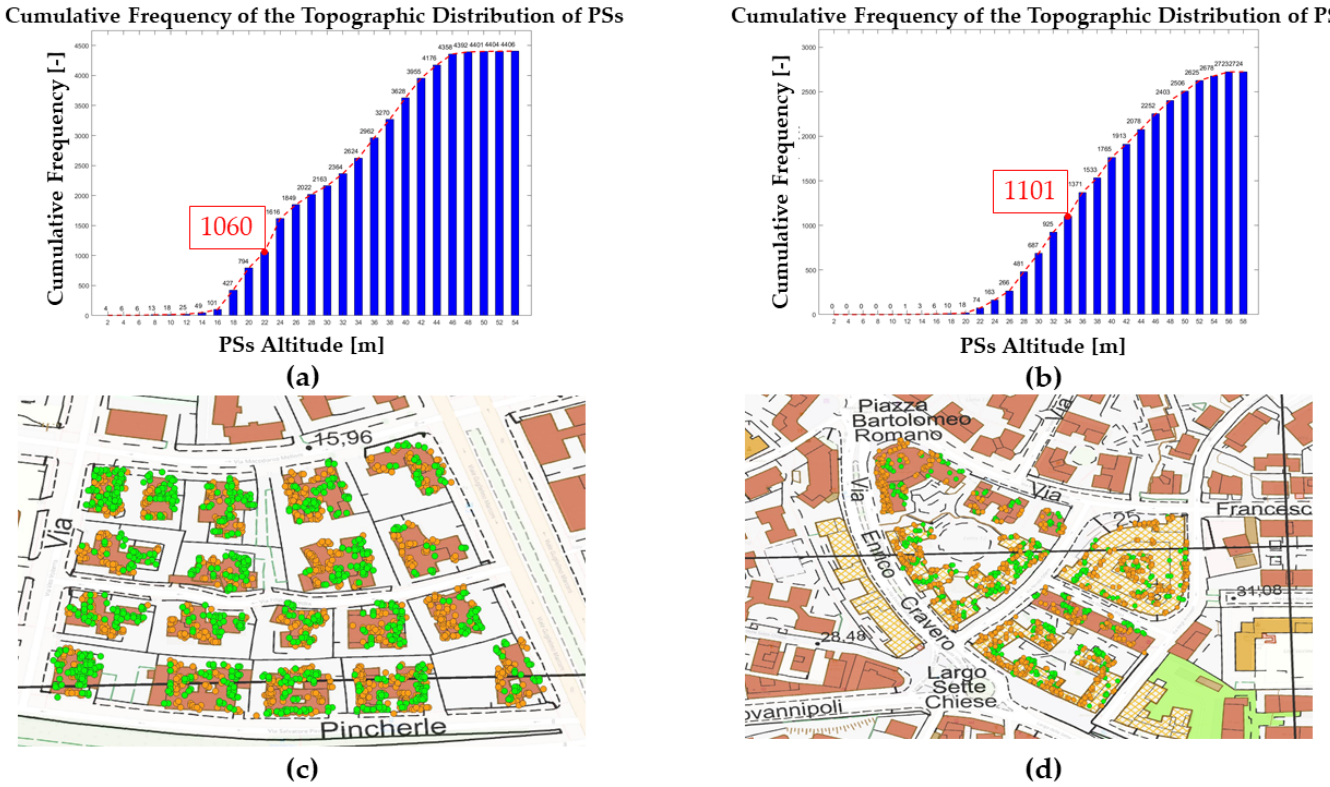

Figure 3. Topographic cumulative distribution of PSs for Area 1 (**a**) and Area 2 (**b**). The red dots indicate the cut-off height δ. The results with removed PSs are shown in (**c**,**d**), respectively.

Figure 4a,b superimpose the PSs to the actual map view by showing the overall view of the buildings with the points that belong to them (marked with different colours). Figure 4c,d report the results of the HC applied to the selected PSs.

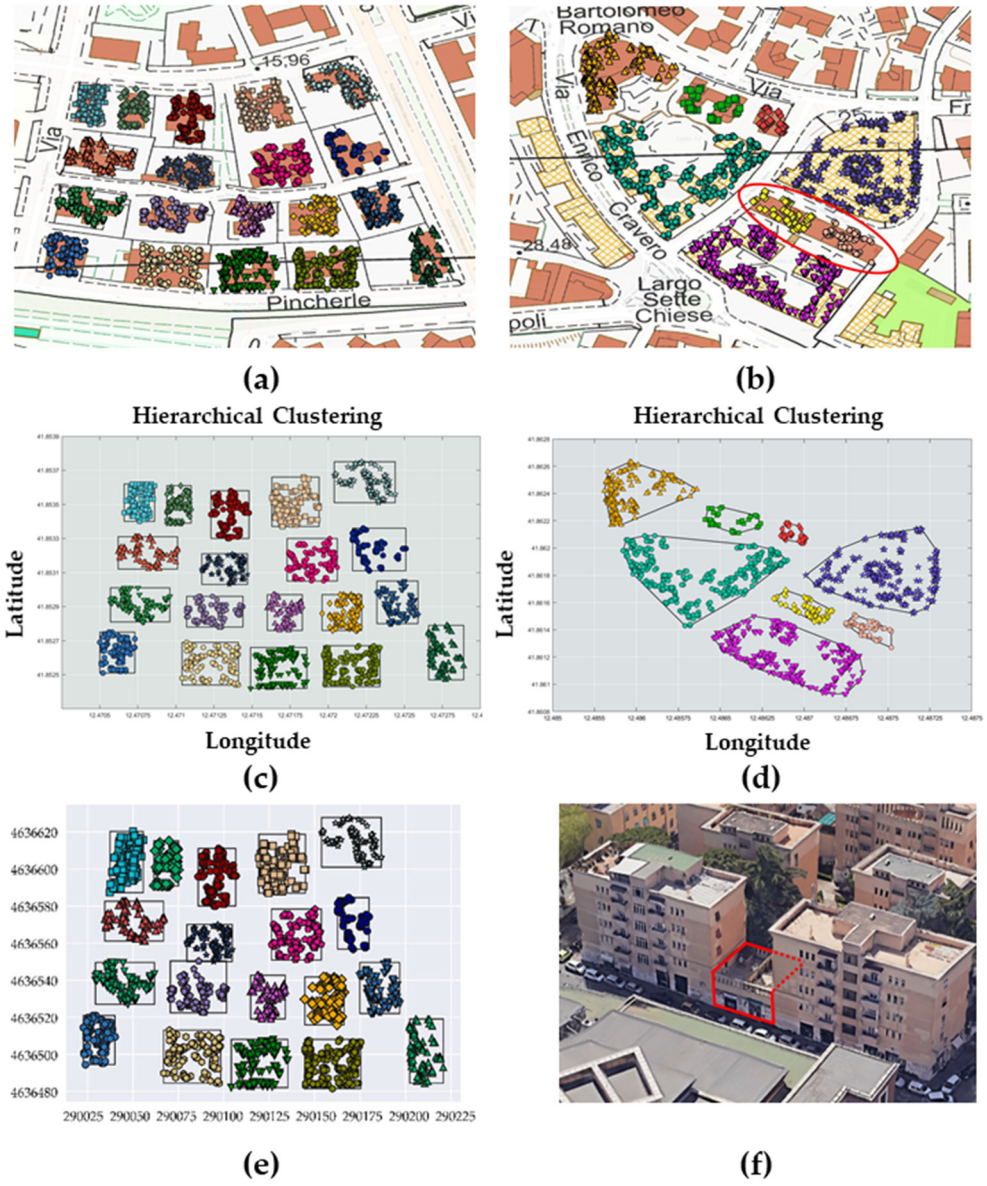

Figure 4. Buildings as identified via Hierarchical Clustering for Area 1 (**c**) and Area 2 (**d**), also superimposed to the QGIS map in (**a**,**b**), respectively. (**e**) Results for the same Area 1 as retrieved from [8]. (**f**) 3D view of the detail marked in red in (**b**).

More specifically, Figure 4c shows (in Area 1) an automatic rectangular shape approach, similar to what was reported in [8]. This more conventional technique fits well with the specificities of this first case study, as most buildings have a regular square or rectangular plan.

Instead, Figure 4d shows a more advanced approach, with the plan view shape not dictated a priori but instead inferred from the datapoints themselves. This is achieved by automatically encircling the most external elements belonging to the same cluster. This automatic shape-finding approach returns very accurate results, considering the peculiarities of this second case study.

As shown in Figure 4a, all the structures in Area 1 are correctly located, and their overall shape is correctly guessed. On the other hand, in Area 2, eight clusters appear instead of the expected seven. Indeed, the structure highlighted by the red ellipse in Figure 4b is misidentified as two detached buildings. The motivation is clearly visible in the 3D view of the building complex (Figure 4f). The small, two-story high portion

enclosed between the two larger, seven-story high side parts reflected very few PSs, making it almost invisible to the satellite. This aspect, unfortunately, constitutes one of the inherent and unavoidable limitations of using satellite data. The complexity and diversity of the environments observed can often generate challenges in the process of data acquisition and interpretation, with phenomena such as shadows generated by adjacent structures that can reduce the reliability and completeness of the information obtained.

To conclude, Figure 4e reports the results of the first area as retrieved from [8], i.e., with the previously proposed DBSCAN-based approach. From a direct comparison of the results on Area 1, it is possible to appreciate how the proposed HC-based approach and the previous DBSCAN-based algorithm returned similar identifications, both consistent with the expected results.

An additional approach explored was the reduction of the cut-off height δ. However, lowering the cut-off value risks including some points associated with the ground surface between buildings, thus complicating the clustering process.

In fact, adopting a cut-off height of 32 m (i.e., 34 m–2 m) resulted in an incoherent clustering outcome due to the excessive inclusion of points referring to the ground surface. Conversely, using a cut-off height of 34 m made it possible to include the few points related to the two-story section enclosed between the taller side parts, allowing the clustering process to correctly identify the entire building as a single cluster, thereby improving the overall accuracy of the model.

Lowering the cut-off height allowed for resolving the issue of cluster separation, as shown in Figure 4b. However, this choice also led to including points associated with the ground rather than the buildings. This is clearly visible in Figure 5b, where some points located on the street are included in the cluster marked by red diamonds and the one indicated by purple triangles.

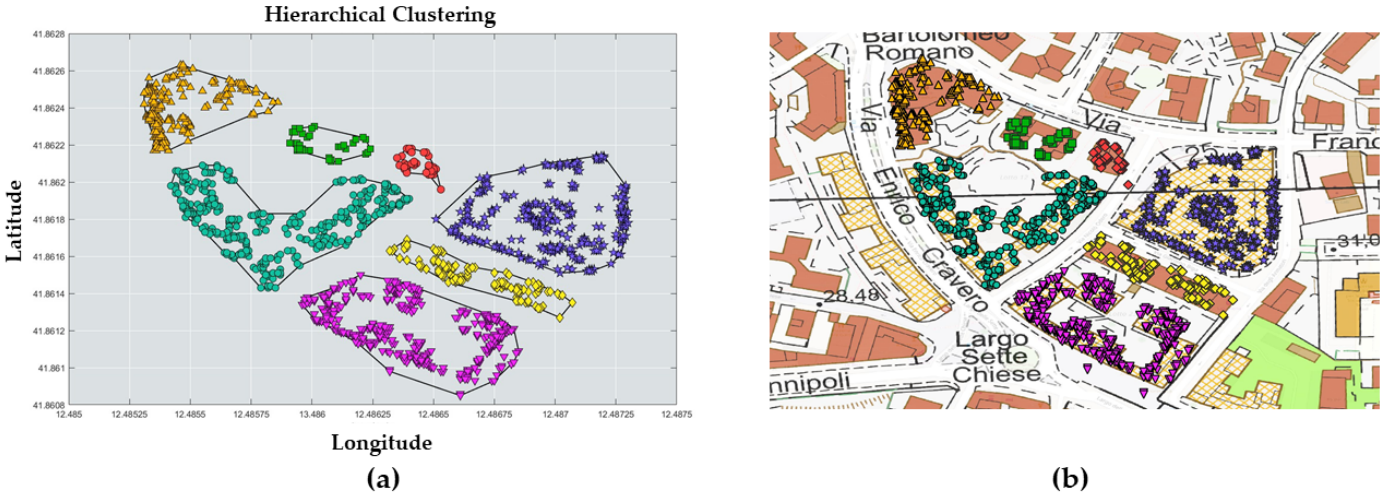

Figure 5. Buildings as identified via Hierarchical Clustering for Area 2 (**a**), also superimposed to the QGIS map in (**b**) using a cut-off height δ of 34 m.

This case represents an uncommon configuration, where a low-rise building is situated between two significantly taller structures. Therefore, in such circumstances, it is necessary to accept the compromise of including some ground-related points in the analysis to ensure the accurate identification of the buildings.

The approach is based on using the maximum first derivative, indicative of the maximum local variation, for determining the cut-off height, which provides sufficiently accurate results in cases where the analysed area exhibits limited elevation differences and is char-

acterised by multi-story buildings. Under such conditions, the cut-off height value is applicable with good approximation to each point within the examined area.

A more accurate solution for determining the cut-off height is by using a digital terrain model (DTM), which provides a detailed three-dimensional representation of the earth's surface. The DTM allows for a more precise capture of elevation variations, thereby enhancing the accuracy of measurements in areas characterised by complex or heterogeneous topographies. In particular, by knowing the topographic value associated with each PS and subtracting the ground altitude provided by the DTM, it is possible to obtain the relative topographic value, which represents the height of the point relative to the ground. This methodology significantly improves the reliability of the results by reducing the noise associated with PSs belonging to the ground.

Although not explored in depth in this article, a different approach utilising the digital terrain model (DTM) may offer interesting insights for future research. It could contribute to further improving the accuracy of results, particularly in complex topographic contexts.

5. Building Prioritisation Results

At this step, each cluster—which, it should be reminded, contains data points collected from both ascending and descending orbits—was proven to correctly correspond to an individual building.

Having achieved the first main goal of this research work (building shape definition), the next step involved selecting the structure that required in situ investigation with the highest priority. In this context, a first ranking criterion is proposed based on differential subsidence and the potential distortion induced by this phenomenon. Then, a second, complementary criterion, based instead on the total average displacements, is also reported and discussed. The advantages and limitations of both strategies are discussed.

It is important to note that both the proposed ranking methodologies compare each building's current state with that of the other buildings in the same area. That is, they do not compare a building's current state with its previous condition, such as in the procedures for early warning and risk assessment proposed by, e.g., [23,24].

For both strategies, it is firstly necessary to calculate the Up–Down (U-D) and East–West (E-W) components of velocities (from now on, V_{UD} and V_{EW}). This can be achieved by considering pairs of data points from ascending and descending orbits. Therefore, the data points need to be paired or omitted if pairing is not possible. Note that the N-S component is intentionally omitted here since the SAR sensor is not quite sensitive to the measurement of the components along this direction due to the lateral view and the near-polar orbit trajectories of the satellite system [10]. Nevertheless, this is known to result in a limited error in the approximation. In this sense, an initial analysis of the relative distances between all the PSs from the two orbits was conducted to make a preliminary selection. Specifically, the data obtained from the Italian COSMO-SkyMed satellite constellation have known precision values: 1–2 m in the N-S direction, 2–3 m in the E-W direction, and 1–2 m in the U-D (vertical) direction, as discussed in more detail in [10]. Therefore, datapoint pairs with planimetric and altimetric distances exceeding these specified error values must be excluded, while all others can be retained for the subsequent operations.

For these remaining datapoint pairs, the velocity values V_{UD} and V_{EW} were calculated by inverting the following simplified relationships [10]:

$$\begin{cases} v_{ASC} \cong v_{EW,ASC} \cdot n_{EW,ASC} + v_{UD} \cdot n_{UD,ASC} \\ v_{DES} \cong v_{EW,DES} \cdot n_{EW,DES} + v_{UD} \cdot n_{UD,DES} \end{cases} \quad (1)$$

where $n_{EW,ASC}$, $n_{UD,ASC}$, $n_{EW,DES}$, and $n_{UD,DES}$ are the directional cosines of the sensor line of sight (LOS). As mentioned, this relationship holds for pairs of spatially coincident ascending orbit (ASC) and descending orbit (DES) points.

At this step, the values can be averaged. The resulting mean is then associated with a new point, which does not correspond to either of the two original PSs in the pair but is instead located at an intermediate coordinate between them.

For what concerns Area 1, Figure 6a,b report these results for, respectively, the U-D and E-W mean velocities. As can be seen from Figure 6c,d, the comparison with the results of the DBSCAN approach retrieved from [8] is remarkable, especially considering that the criterion for selecting points related to buildings is slightly different, as the approach used in [8] employed the DTM to determine the cut-off height.

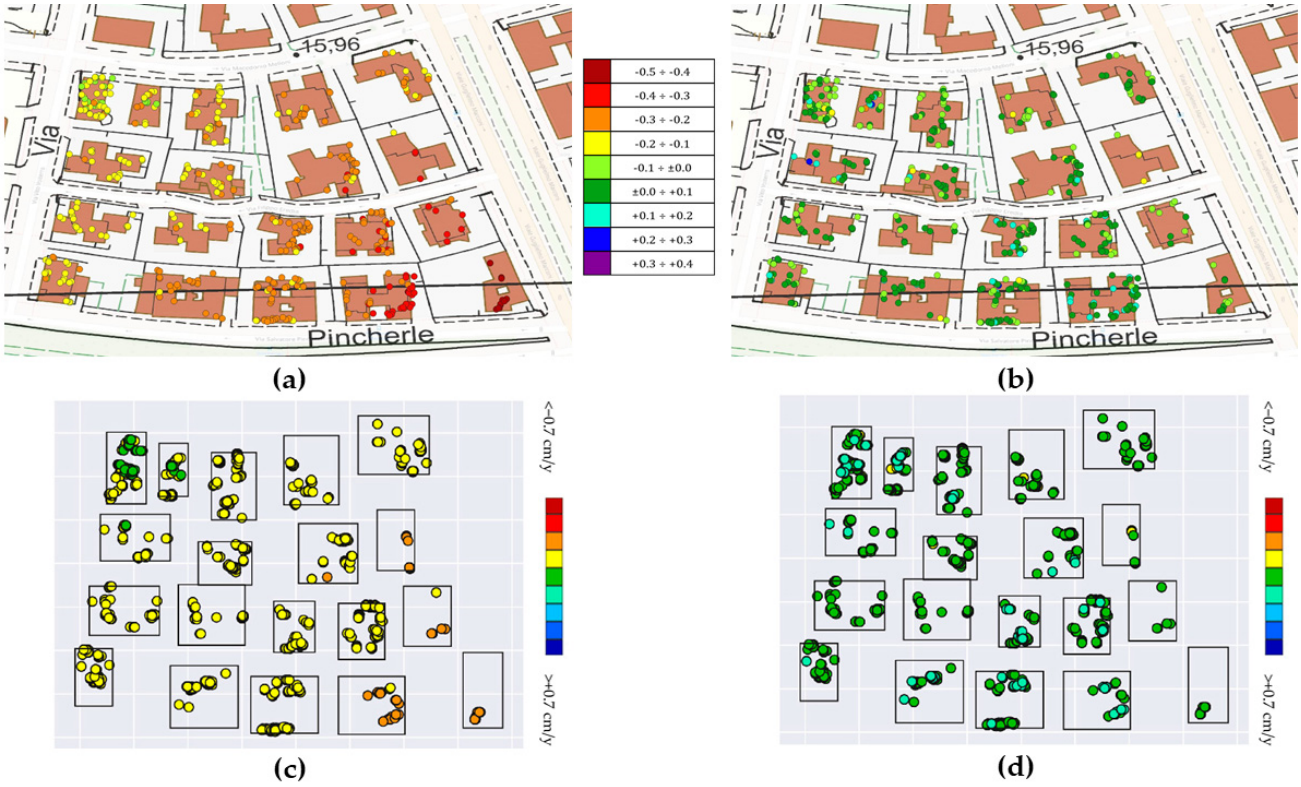

Figure 6. Selection of the most at-risk building in Area 1: (**a**) mean values of V_{UD} (for the selected pairs of data points); (**b**) mean values of v_{EW}. The colour legend is in cm/year. Results from Ref [8] are shown in (**c**,**d**) for direct comparability.

This analysis indicates an ongoing deformation phenomenon in Area 1, characterised predominantly by U-D displacements (more specifically, by a downward movement). This displacement is more pronounced in the SE corner of the map and diminishes moving toward the NW corner. This pattern is attributed to subsidence, a geological process involving the slow and gradual sinking of the soil. These findings are consistent with those of [8], though are not detailed here for brevity.

From the perspective of structural integrity, downward rigid roto-translation is not inherently the most critical issue. Differential displacements are a more accurate indicator of structural risk, as they induce strain within the structure, potentially causing damage. Therefore, the maximum and minimum velocity components in the E-W ($V_{EW,max}$, $V_{EW,min}$) and vertical ($V_{UD,max}$, $V_{UD,min}$) directions were considered for each cluster. The second case is more critical due to the larger displacements. From this enhanced analysis, the second

building from the left in the first row from the top was identified as the one exhibiting the highest differential total displacements.

Conversely, the last building of the fourth row experiences the lowest level of total differential displacement. Interestingly, the building at the highest risk is located in the area with the least sinking (upper left corner), while the one with the least differential displacements is in the region with the highest total subsidence (lower right corner).

These observations confirm that a global analysis of deformations, even using remotely sensed satellite data, can provide a comprehensive overview of the expected behaviour of target structures and identify potentially hazardous situations. This approach can help prioritise in situ surveys and offer valuable information for integrating detailed studies of buildings in the area.

For what concern Area 2, Figure 7a,b report the results according to the same conventions seen in Figure 6.

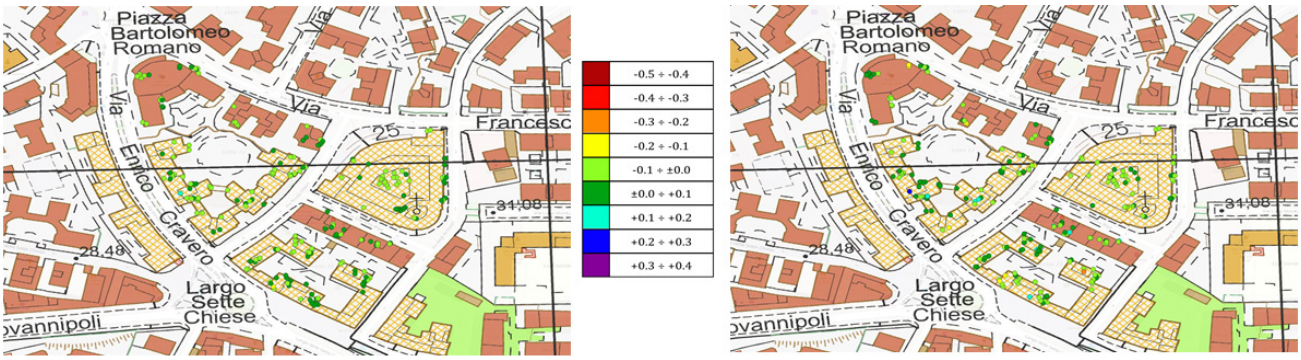

Figure 7. Selection of the most at-risk building in Area 2: (**a**) mean values of V_{UD} (for the selected pairs of data points); (**b**) mean values of v_{EW}. The colour legend is in cm/year.

First of all, it is possible to observe that this second area is subjected to much less intense rigid motion, especially in the vertical direction. That is to say, it is not as significantly affected by subsidence phenomena. In this case, the large V-shaped building in the centre of the inspected area is the one affected by the (relatively) highest differential displacements, while the triangular-shaped building in the upper right is the one less affected.

As already mentioned before, to complement the previous analysis, a study was conducted to establish an internal priority list, also assigning a level of attention to each building in the analysed area. To facilitate data management, each building was assigned an identification code, as shown in Figure 8a,b, which pertain respectively to Area 1 and Area 2.

5.1. Distortion-Based Priority Ranking

The first proposed strategy involves, after acquiring the vertical velocity values (V_{UD}), calculating a distortion index for each building. That is here defined as the difference between the maximum ($V_{UD,max}$) and minimum ($V_{UD,min}$) values of V_{UD}, normalised by the length (L), which represents the physical distance between the corresponding measurement points:

$$D = \frac{\Delta V_{UD}}{L} = \frac{V_{UD,max} - V_{UD,min}}{L} \quad (2)$$

This index measures the variation of vertical displacement over the spatial separation between the considered points, providing a detailed assessment of the degree of deformation experienced by the buildings. The more stable the trend of the DInSAR displacements is, the more precise will be the proposed approach. The results of this methodology are

shown in Figure 8c,d. It should be remarked that this normalisation in itself may not guarantee the identification of the actual maximum value of the distortion. However, this approach constitutes a necessary assumption for implementing a method that offers a quantitative and valuable parameter for an initial assessment of the priority level while remaining computationally efficient. The alternative would be to examine all possible combinations of distances and vertical velocity differences between the points of each building; however, this task would be significantly more complex and computationally demanding for large areas.

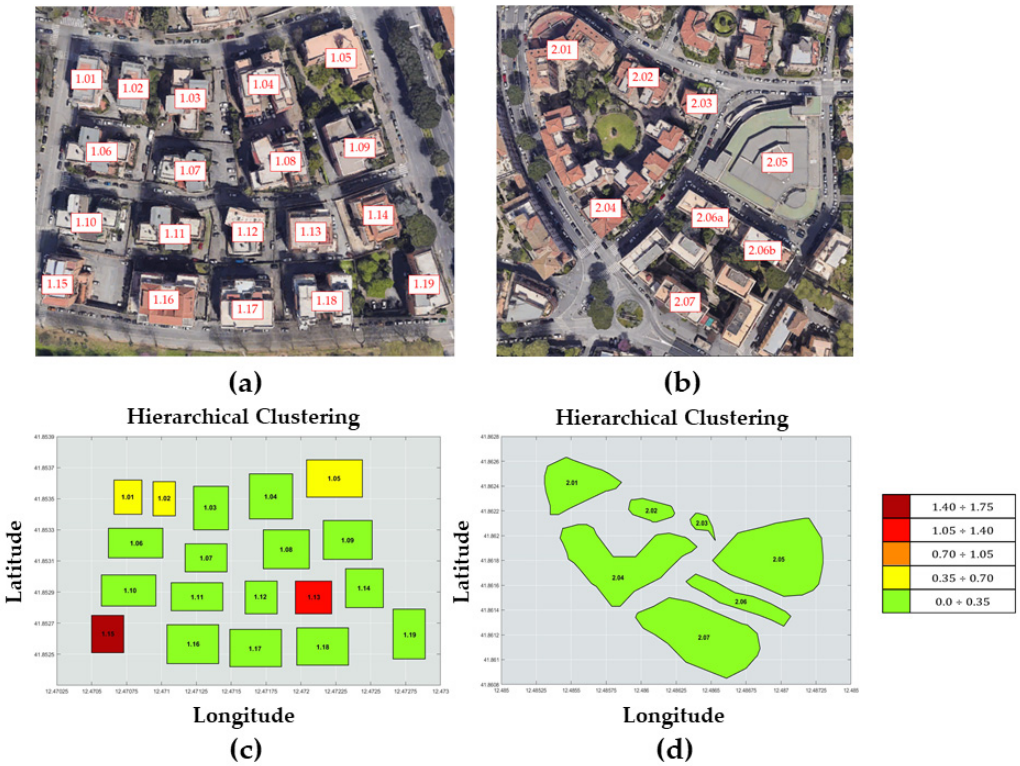

Figure 8. ID codes assigned to each building in (**a**) Area 1 and (**b**) Area 2 for the priority list. The absolute value of the distortion index corresponding to the buildings in Area 1 (**c**) and Area 2 (**d**). The colour legend is in ‰.

Once the distortion index was determined, a classification was applied, based on the sum of the mean (μ_{DI}) and standard deviation ($-\sigma_{DI}$) of the distortion index for each area. This method is commonly used to identify values that significantly deviate from the trend of the analysed population; assuming a normal distribution, it corresponds to a confidence interval of circa 84%. Buildings with a distortion index exceeding the threshold value were classified as buildings requiring a higher level of attention, marked with an * next to the Priority Rank. This classification highlights, in relative terms, the buildings within the area that require more attention than the others (independently of the global risk level of the whole inspected area). Table 1 reports the mean (μ_{DI}) and standard deviation ($-\sigma_{DI}$) values for the two analysed areas.

Table 1. Mean (μ_{DI}) and standard deviation ($-\sigma_{DI}$) values of the distortion index for buildings in Areas 1 and 2 (values in cm/y).

Area	μ_{DI}	$-\sigma_{DI}$	Threshold
1	−0.30	−0.46	−0.76
2	−0.14	−0.09	−0.23

In general, it is possible that using the standard deviation may result in some false positives or false negatives. However, given the specific nature of the data available, it remains the most suitable and feasible approach for our case. Establishing specific absolute thresholds is too dependent on other parameters like the structural types of the buildings.

Tables 2 and 3, pertaining respectively to Area 1 and Area 2, present the results of this analysis, ordered in descending order of distortion (and, therefore, of priority). Unfortunately, no benchmark or target value is available, as the buildings are not instrumented with physically attached sensors. However, it is well known from different works in the literature [20,22] that the displacements found are absolutely compatible with the presence of a subsidence phenomenon that has been ongoing for many years in the area.

Table 2. Distortion index and Priority Ranks for buildings in Area 1, including vertical velocity measurements (values in cm/y, length in metres, distortion index in ‰). The * marks building exceeding the threshold value and thus classified as requiring a higher level of attention.

ID Cluster	$V_{UD,max}$	$V_{UD,min}$	ΔV_{UD}	L	Distortion Index (‰)	Priority Rank
1.15	−0.26	−0.07	−0.19	1.09	−1.68	1 *
1.13	−0.32	−0.17	−0.15	1.09	−1.38	2 *
1.01	−0.23	−0.07	−0.16	3.30	−0.50	3
1.05	−0.27	−0.17	−0.10	1.97	−0.49	4
1.02	−0.28	−0.03	−0.25	5.97	−0.43	5
1.08	−0.35	−0.16	−0.19	7.89	−0.25	6
1.04	−0.26	−0.16	−0.10	5.83	−0.17	7
1.17	−0.32	−0.16	−0.16	11.42	−0.14	8
1.03	−0.24	−0.11	−0.13	12.74	−0.10	9
1.07	−0.22	−0.14	−0.08	8.62	−0.10	10
1.10	−0.19	−0.11	−0.08	9.04	−0.08	11
1.12	−0.34	−0.19	−0.15	18.55	−0.08	12
1.06	−0.24	−0.11	−0.13	20.37	−0.06	13
1.09	−0.35	−0.18	−0.17	28.38	−0.06	14
1.14	−0.36	−0.24	−0.12	20.52	−0.06	15
1.18	−0.40	−0.24	−0.16	35.37	−0.05	16
1.11	−0.25	−0.13	−0.12	31.81	−0.04	17
1.16	−0.29	−0.17	−0.12	36.85	−0.03	18
1.19	−0.47	−0.42	−0.05	20.98	−0.02	19

Table 3. Distortion index and Priority Ranks for buildings in Area 2, including vertical velocity measurements (values in cm/y, length in metres, distortion index in ‰). The * marks building exceeding the threshold value and thus classified as requiring a higher level of attention.

ID Cluster	$v_{UD,max}$	$v_{UD,min}$	ΔV_{UD}	L	Distortion Index	Priority Rank
2.07	−0.11	0.10	−0.21	6.37	−0.33	1 *
2.04	0.16	−0.11	0.27	14.41	0.18	2
2.05	−0.10	−0.04	−0.06	3.53	−0.17	3
2.03	0.07	−0.03	0.10	9.64	0.10	4
2.02	0.09	−0.07	0.16	18.59	0.08	5
2.01	0.07	−0.06	0.13	28.43	0.05	6
2.06	0.09	−0.06	0.15	35.53	0.04	7

The analysis of the two areas reveals significant differences in terms of deformative behaviour and building vulnerability. Area 1 exhibits more pronounced settlement values than Area 2, with values reaching −0.47 cm/year, indicating a more marked subsidence

phenomenon. This translates into higher distortion indices relative to Area 2, where vertical velocities are more moderate.

The proposed approach allowed the identification of two buildings in Area 1, designated by ID numbers 1.13 and 1.15, and one in Area 2, identified by ID number 2.07, with the highest priority level. Once more, it is essential to recall and emphasise that the priority level is assessed in relative terms within each area: a building with a maximum attention level requires greater attention compared to other buildings in the same area without necessarily implying an absolute criticality. In other words, the analysis highlights the structures that need priority monitoring within the local context rather than making a direct comparison between different areas, thereby contributing to the optimisation of resources and mitigation actions.

The results obtained for Area 1 show a variation in vertical velocities of about -2 mm/year over short distances of 1.09 m. To verify the reliability of these findings, a statistical test was performed to identify potential outliers, analysing the differences in vertical velocities (ΔV_{UD}) between the maximum and minimum values, as well as the lengths (L). With a 90% confidence interval, the test identified a single outlier, which does not correspond to the two main clusters (1.15 and 1.13), which show differential settlements of -1.9 and -1.5 mm/year over distances of 1.09 m.

As shown in Figure 9a, related to Area 1, these results indicate that the obtained value is not an outlier and, therefore, the data are statistically valid. Moreover, the same test was also replicated for Area 2, as shown in Figure 9b, where, with a 90% confidence interval, no outliers were identified.

From a scientific perspective, this deformation rate could be consistent with the onset of a subsidence phenomenon, which, although having a relatively low magnitude, might manifest over limited areas with significant effects on vertical ground deformation [25].

In this context, the observed phenomenon aligns with the findings of Stramondo et al. [21], who conducted a study on the surface movements of buildings and urban structures in the city of Rome. Their work highlighted subsidence phenomena of modest magnitude yet very localised, causing significant vertical deformations and differential settlement similar to those found in the analysed area.

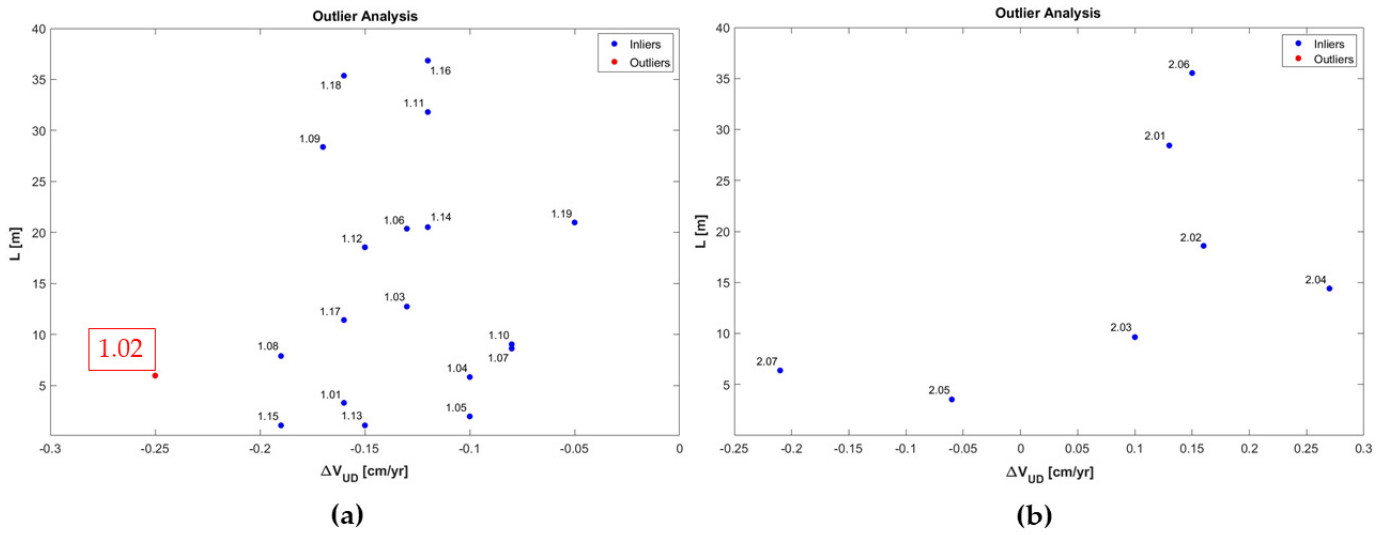

Figure 9. Statistical analysis of vertical velocity variation for Area 1 (**a**) and Area 2 (**b**).

However, it is also important to highlight that, according to the inspected sources (http://www.urbanistica.comune.roma.it/images/citta-15-minuti/15min-VIII-mun.pdf; last accessed 20 December 2024; Italian only), several buildings in this area have recently

undergone renovation, making it challenging to determine any damage directly associated with the observed deformations.

It is also crucial to consider that this distortion could also result from errors related to the accuracy of InSAR data. Although InSAR is widely used for large-scale deformation monitoring, it is subject to inherent limitations such as spatial resolution and uncertainties arising from the separation between measurement points. These errors can cause distortions in the results that do not necessarily reflect the physical reality of the ground. Additionally, the lack of ground-based instrumentation for data validation makes it challenging to verify the true nature of the observed distortion, whether due to a subsidence phenomenon or inaccuracies in the measurement of deformations. Therefore, the results should be interpreted as a preliminary indication rather than a definitive assessment of the site conditions.

Despite these potential uncertainties, the methodology was designed to provide a preliminary and scalable assessment of the at-risk areas. This means that the methodology is intended to address large areas, offering an initial screening of potentially vulnerable buildings to direct resources and monitor actions to less prioritised structures. Although the method may present issues, particularly for isolated buildings or areas with more complex deformation phenomena, it still provides a valuable tool for rapidly identifying structures requiring more in-depth evaluation.

This classification methodology based on the relationship between angular distortion and risk or damage shares some conceptual similarities with approaches proposed in previous studies. For instance, Sanabria et al. [26] introduced a system to classify buildings based on their structural damage level—negligible, medium, and high—using the maximum differential settlement and the maximum angular distortion along the line of sight (LOS). Although this approach provides valuable insights for assessing structural vulnerability, its application to the present study would require the availability of cumulative displacement data, which are not available in our case, where the assessment is based on the distortion index calculated for individual buildings using vertical velocity measurements.

On the other hand, Milillo et al. [27] developed a methodology to assess structural damage induced by tunnelling, based on greenfield settlement models (in the absence of buildings), deflection ratios (Δ/L), and a modification factor (MF) to account for the soil–structure interaction. However, since this method refers to ground-based points rather than building-specific data, it does not apply to the context of our study.

Finally, the differential subsidence approach discussed by Cigna and Tapete [28] offers a complementary perspective by using subsidence gradients and angular distortions to identify risk areas for urban infrastructures. While helpful in characterising rapid transitions between different soil types (soft or solid) and the associated surface fault risks, this methodology focuses on ground characteristics rather than direct building deformations, thus differentiating it from our approach, which considers the distortion index on a building scale. Other noteworthy examples may include the differential deformation maps proposed by Ezquerro et al. [29] or, very recently, Shahbazi et al. [30]. However, all these approaches are potentially subject to the same issues encountered here, i.e., potential excessive distortions due to single-point measurement errors.

5.2. Total Average Subsidence-Based Priority Ranking

In addition to the classification previously described, a second classification is considered and reported. This alternative and complementary ranking considers other potential damaging mechanisms and is based on the average vertical velocity ($V_{UD,av}$) for each building. This approach was performed both for comparative purposes, to compare the results obtained with those of the classification based on the maximum and minimum vertical velocity values,

and to provide a complementary view of structural behaviour over time, offering a more balanced perspective of different damaging mechanisms caused by soil deformation.

The average deformation velocity ($V_{UD,av}$) for each building is calculated as the mean of the vertical velocity (V_{UD}) values recorded at the different measurement points corresponding to the building. This approach distinguishes itself from the previous analysis, which was based on maximum and minimum values that, while providing useful indications, might be influenced by temporary or localised phenomena. In contrast, the average velocity allows for consideration of the overall deformation trend over time, reducing the impact of isolated value peaks that do not reflect the overall behaviour of the structure.

Although differential settlements represent a higher risk to the safety of the buildings, absolute settlement, while not immediately hazardous, may signal the presence of widespread subsidence phenomena that could, over time, affect the functionality and stability of the structures.

In this context, buildings with $V_{UD,av}$ values exceeding a defined threshold are considered to have a higher level of attention. This threshold is established based on the sum of the mean (μ_{AVV}) and standard deviation ($-\sigma_{AVV}$) of each area's average velocity values, using a methodology similar to that employed for the distortion index-based classification. Buildings with an average velocity exceeding this threshold are labelled as "high priority" for monitoring, as their deformation may evolve into more serious issues over time if not adequately tracked. The mean (μ_{AVV}) and standard deviation ($-\sigma_{AVV}$) values for the two analysed areas are reported in Table 4. According to these thresholds, the high-priority buildings are indicated in Tables 5 and 6 with an * next to their respective level.

Table 4. Mean (μ_{AVV}) and standard deviation (σ_{AVV}) values of the average vertical velocity in Areas 1 and 2 (values in cm/y).

Area	μ_{AVV}	$-\sigma_{AVV}$	Threshold
1	−0.23	−0.07	−0.30
2	−0.01	−0.02	−0.03

Table 5. Priority Rank for buildings in Area 1 based on average vertical velocity (in cm/year). The * marks building exceeding the threshold value and thus classified as requiring a higher level of attention.

ID Cluster	$V_{UD,av}$	Priority Rank
1.19	−0.44	1 *
1.18	−0.32	2 *
1.14	−0.31	3 *
1.09	−0.29	4
1.13	−0.28	5
1.08	−0.26	6
1.12	−0.26	7
1.16	−0.24	8
1.17	−0.23	9
1.05	−0.22	10
1.04	−0.22	11
1.11	−0.20	12
1.07	−0.19	13
1.03	−0.19	14
1.15	−0.18	15
1.10	−0.16	16
1.06	−0.15	17
1.02	−0.15	18
1.01	−0.13	19

Table 6. Priority Rank for buildings in Area 2 based on average vertical velocity (in cm/year). The * mark building exceeding the threshold value and thus classified as requiring a higher level of attention.

ID Cluster	$V_{UD,av}$	Priority Rank
2.05	−0.07	1 *
2.03	0.01	2
2.01	−0.01	3
2.06	0.00	4
2.02	0.00	5
2.07	0.00	6
2.04	0.00	7

Adopting this additional classification thus enriches the overall analysis, providing another complementary tool for planning and implementing prevention and mitigation actions. The combination of the two approaches—analysis based on the distortion index and the analysis of average velocity—offers a comprehensive view of structural health, as well as a valuable contribution to resource management and the prioritisation of interventions in the monitored areas.

The average deformation velocity ($V_{UD,av}$) values recorded for Area 2 are significantly lower than those of Area 1, indicating a higher overall stability of the region, as previously observed in Figure 6a,b, respectively, for Area 1 and Area 2. Specifically, the majority of the clusters in Area 2 exhibit velocity values close to zero, indicating minimal or no settlement. This behaviour suggests that deformations over time are extremely limited, with any potential subsidence phenomena being negligible or virtually non-existent.

This second approach, based on average velocities, allowed for the identification of three buildings in Area 1, designated by the ID numbers 1.19, 1.18, and 1.14, and one building in Area 2, identified by the ID number 2.05, with the highest level of attention needed.

To summarise, the distortion-based priority ranking presented in Section 5.1 highlighted two buildings in Area 1 and one in Area 2 that have higher-than-expected distortion indices (yet not high enough to be seen as unrealistic statistical outliers). Instead, the total average subsidence-based priority ranking presented here in Section 5.2 identified another set of buildings (three in Area 1 and one in Area 2) that exhibit high average deformation velocity. This second classification provides an additional tool to optimise the management of priorities. It may ensure that buildings with uniform and relatively less severe settlements that are potentially evolving into structural issues over the long term are also closely monitored.

The next steps in preventive maintenance for these highest-priority buildings would be to arrange in situ surveys in the near future, listing the target buildings for periodic checks, and, if needed, the installation of an array of physically attached sensors for permanent and continuous monitoring. However, these next steps fall outside this paper's scope and will be addressed in future analyses.

6. Conclusions

The issue of the interpretation of structural behaviour following the processing of satellite data is of fundamental importance, also in relation to the types of actions whose effects on structures can be effectively monitored using interferometric techniques. It is, in fact, evident that satellite data, the frequency of which depends on the passage of the satellite over the area of interest and varies from a few days to a few weeks, provide good results in the case of the observation of slowly evolving phenomena. In contrast, they are currently less effective for evaluating phenomena whose evolution may be faster.

During their useful life, constructions interact first and foremost with the geological and environmental context in which they are built. Consequently, in addition to gravity loads and earthquakes, constructions are also subject to additional actions induced on the structure by environmental, meteorological, and subsurface instability phenomena, which are independent of the presence of the structure itself and which can, in any case, generate displacements in the structure that can also be monitored using the interferometric technique. Therefore, to obtain an overall view of the actions that can determine movements that can be monitored by satellite interferometry, it is important to know, on the one hand, the characteristics of the structure and, on the other hand, the geological context of the subsoil and the environmental context in which the construction itself is inserted.

This contribution reports the results of a newly proposed approach for satellite data-based Structural Health Monitoring. This proposal combines machine learning and Knowledge Extraction to automatically identify civil buildings, estimate their shapes in the plan view, and select the ones most likely at risk of damage due to ground subsidence. In particular, the methodology developed and presented here integrates remote sensing measurements (Persistent Scatterers in SBAS-DInSAR products) and the unsupervised learning technique known as Hierarchical Clustering. This clustering process enables the automatic recognition and grouping of buildings based on their deformation patterns. The proposed algorithm was successfully applied to two specific areas in Rome, Italy, using data from the COSMO-SkyMed SAR satellite constellation over the 2011–2019 period.

Two methodologies are presented and proposed for building prioritisation: a first one, based on differential subsidence and distortion, and a second one, based on total subsidence velocity. They can be seen as complementary approaches for assessing the structural vulnerabilities of the monitored buildings. The analysis of the distortion index enables the identification of buildings characterised by significant localised deformations, providing an effective tool for highlighting issues related to structural stability. In contrast, the approach based on the average vertical velocity offers a comprehensive perspective on the deformation behaviour over time, proving particularly useful for detecting large-scale subsidence phenomena and identifying buildings susceptible to significant settlements.

These approaches allowed for the definition and comparison of two distinct internal priority rankings for interventions, assigning each building a relative level of attention. This method optimises the use of resources for field monitoring and facilitates the identification of the most critical points destined for further investigation. However, the two procedures yielded different results, highlighting how different damage mechanisms may affect distinct areas. Specifically, buildings 1.13, 1.15, and 2.07 appear more at risk of distortion-induced damage, while buildings 1.14, 1.18, 1.19, and 2.05 seem more at risk of total subsidence.

In conclusion, integrating satellite interferometric techniques and machine learning algorithms represents a significant advancement in the structural monitoring of urban areas. The proposed methodology, capable of automatically identifying buildings and prioritising those at greater risk, is an effective tool to support the planning of mitigation and preventive maintenance interventions. Future works will further assess the capabilities of this promising technique to select and prioritise critical constructions within complicated built environments.

Author Contributions: Conceptualisation, M.C., A.M., A.P. and B.C.; methodology, M.C. and A.M.; software, Y.H., M.C. and A.M.; validation, Y.H., M.C. and A.M.; formal analysis, Y.H., M.C. and A.M.; resources, M.B.; data curation, M.B.; writing—original draft preparation, Y.H., M.C. and A.M.; writing—review and editing, A.P., F.F. and B.C.; visualisation, Y.H., M.C. and A.M.; supervision, A.P., F.F. and B.C.; project administration, A.P., F.F. and B.C.; funding acquisition, A.P. and B.C. All authors have read and agreed to the published version of the manuscript.

Funding: This work was supported by the Italian Civil Protection Department (DPC) and the I-AMICA (PONa3_00363) project. This research was carried out in the framework of the research agreement between the Italian Civil Protection Department (DPC) and the "Istituto per il Rilevamento Elettromagnetico dell'Ambiente"—National Research Council (IREA-CNR) and was partially funded by the Italian Civil Protection Department within the project RELUIS 2019–2022 WP6 "Structural Health Monitoring and Satellite Data". MC and BC are financially supported by the PNRR project CN MOST SPOKE 7—WP4 " Resilience of networks, structural health monitoring and asset management". This work was carried out using CSK® Products, © of the Italian Space Agency (ASI), delivered under a license to use by ASI. The Digital Elevation Model of the analysed area was acquired through the SRTM archive.

Data Availability Statement: The satellite data used for this investigation were provided by Istituto per il Rilevamento Elettromagnetico dell'Ambiente"—National Research Council (IREA-CNR).

Conflicts of Interest: The authors declare no conflicts of interest.

References

1. Miano, A.; Mele, A.; Calcaterra, D.; Martire, D.D.; Infante, D.; Prota, A.; Ramondini, M. The Use of Satellite Data to Support the Structural Health Monitoring in Areas Affected by Slow-Moving Landslides: A Potential Application to Reinforced Concrete Buildings. *Struct. Health Monit.* **2021**, *20*, 3265–3287. [CrossRef]
2. Tonelli, D.; Valentini, A.; Rocca, A.; Zorzi, S.; Lotti, A.; Zonta, D. Uncertainty Quantification of Satellite InSAR-Monitoring of Bridges: A Case Study. *ce/papers* **2023**, *6*, 900–906. [CrossRef]
3. Tonelli, D.; Caspani, V.F.; Valentini, A.; Rocca, A.; Torboli, R.; Vitti, A.; Perissin, D.; Zonta, D. Interpretation of Bridge Health Monitoring Data from Satellite InSAR Technology. *Remote Sens.* **2023**, *15*, 5242. [CrossRef]
4. Ponzo, F.C.; Auletta, G.; Ielpo, P.; Ditommaso, R. DInSAR–SBAS Satellite Monitoring of Infrastructures: How Temperature Affects the "Ponte Della Musica" Case Study. *J. Civ. Struct. Health Monit.* **2024**, *14*, 745–761. [CrossRef]
5. Giordano, P.F.; Turksezer, Z.I.; Previtali, M.; Limongelli, M.P. Damage Detection on a Historic Iron Bridge Using Satellite DInSAR Data. *Struct. Health Monit.* **2022**, *21*, 2291–2311. [CrossRef]
6. Miano, A.; Di Carlo, F.; Mele, A.; Bonano, M.; Prota, A.; Meda, A. Damage Assessment Through the Use of SBAS-DInsar Data: An Application to the "Vittorino Da Feltre" Masonry School Building in Rome. *Int. J. Archit. Herit.* **2023**, *18*, 1077–1096. [CrossRef]
7. Delo, G.; Civera, M.; Lenticchia, E.; Miraglia, G.; Surace, C.; Ceravolo, R. Interferometric Satellite Data in Structural Health Monitoring: An Application to the Effects of the Construction of a Subway Line in the Urban Area of Rome. *Appl. Sci.* **2022**, *12*, 1658. [CrossRef]
8. Mele, A.; Vitiello, A.; Bonano, M.; Miano, A.; Lanari, R.; Acampora, G.; Prota, A. On the Joint Exploitation of Satellite DInSAR Measurements and DBSCAN-Based Techniques for Preliminary Identification and Ranking of Critical Constructions in a Built Environment. *Remote Sens.* **2022**, *14*, 1872. [CrossRef]
9. Mele, A.; Crosetto, M.; Miano, A.; Prota, A. ADAfinder Tool Applied to EGMS Data for the Structural Health Monitoring of Urban Settlements. *Remote Sens.* **2023**, *15*, 324. [CrossRef]
10. Talledo, D.A.; Miano, A.; Bonano, M.; Di Carlo, F.; Lanari, R.; Manunta, M.; Meda, A.; Mele, A.; Prota, A.; Saetta, A.; et al. Satellite Radar Interferometry: Potential and Limitations for Structural Assessment and Monitoring. *J. Build. Eng.* **2022**, *46*, 103756. [CrossRef]
11. Berardino, P.; Fornaro, G.; Lanari, R.; Sansosti, E. A New Algorithm for Surface Deformation Monitoring Based on Small Baseline Differential SAR Interferograms. *IEEE Trans. Geosci. Remote Sens.* **2002**, *40*, 2375–2383. [CrossRef]
12. Bonano, M.; Striano, P.; Yasir, M.; Buonanno, S.; Casu, F.; De Luca, C.; Fusco, A.; Roa, Y.L.B.; Zinno, I.; Virelli, M.; et al. New Advances of the P-SBAS Approach for an Efficient Parallel Processing of Large Volumes of Full-Resolution Multi-Temporal DInSAR Interferograms. *IEEE J. Sel. Top. Appl. Earth Obs. Remote Sens.* **2024**, *18*, 2317–2341. [CrossRef]
13. Casu, F.; Elefante, S.; Imperatore, P.; Zinno, I.; Manunta, M.; De Luca, C.; Lanari, R. SBAS-DInSAR Parallel Processing for Deformation Time-Series Computation. *IEEE J. Sel. Top. Appl. Earth Obs. Remote Sens.* **2014**, *7*, 3285–3296. [CrossRef]
14. Pepe, A.; Berardino, P.; Bonano, M.; Euillades, L.D.; Lanari, R.; Sansosti, E. SBAS-Based Satellite Orbit Correction for the Generation of DInSAR Time-Series: Application to RADARSAT-1 Data. *IEEE Trans. Geosci. Remote Sens.* **2011**, *49*, 5150–5165. [CrossRef]
15. Scifoni, S.; Bonano, M.; Marsella, M.; Sonnessa, A.; Tagliafierro, V.; Manunta, M.; Lanari, R.; Ojha, C.; Sciotti, M. On the Joint Exploitation of Long-Term DInSAR Time Series and Geological Information for the Investigation of Ground Settlements in the Town of Roma (Italy). *Remote Sens. Environ.* **2016**, *182*, 113–127. [CrossRef]
16. Aggarwal, C.C. *Data Mining: The Textbook*; Springer: New York, NY, USA, 2015; ISBN 978-3-319-14141-1.

17. Mugnaini, V.; Zanotti Fragonara, L.; Civera, M. A Machine Learning Approach for Automatic Operational Modal Analysis. *Mech. Syst. Signal Process* **2022**, *170*, 108813. [CrossRef]
18. Civera, M.; Mugnaini, V.; Zanotti Fragonara, L. Machine Learning-Based Automatic Operational Modal Analysis: A Structural Health Monitoring Application to Masonry Arch Bridges. *Struct. Control Health Monit.* **2022**, *29*, e3028. [CrossRef]
19. Di Carlo, F.; Miano, A.; Giannetti, I.; Mele, A.; Bonano, M.; Lanari, R.; Meda, A.; Prota, A. On the Integration of Multi-Temporal Synthetic Aperture Radar Interferometry Products and Historical Surveys Data for Buildings Structural Monitoring. *J. Civ. Struct. Health Monit.* **2021**, *11*, 1429–1447. [CrossRef]
20. Berto, L.; Doria, A.; Saetta, A.; Stella, A.; Talledo, D. Assessment of the Applicability of DInSAR Techniques for Structural Monitoring of Cultural Heritage and Archaeological Sites. *Lect. Notes Civ. Eng.* **2021**, *156*, 691–697. [CrossRef]
21. Stramondo, S.; Bozzano, F.; Marra, F.; Wegmuller, U.; Cinti, F.R.; Moro, M.; Saroli, M. Subsidence Induced by Urbanisation in the City of Rome Detected by Advanced InSAR Technique and Geotechnical Investigations. *Remote Sens. Environ.* **2008**, *112*, 3160–3172. [CrossRef]
22. QGIS Geographic Information System. Available online: https://qgis.Org (accessed on 23 December 2024).
23. Cusson, D.; Rossi, C.; Ozkan, I.F. Early Warning System for the Detection of Unexpected Bridge Displacements from Radar Satellite Data. *J. Civ. Struct. Health Monit.* **2021**, *11*, 189–204. [CrossRef]
24. Guzman-Acevedo, G.M.; Vazquez-Becerra, G.E.; Quintana-Rodriguez, J.A.; Gaxiola-Camacho, J.R.; Anaya-Diaz, M.; Mediano-Martinez, J.C.; Carrión Viramontes, F.J. Structural Health Monitoring and Risk Assessment of Bridges Integrating InSAR and a Calibrated FE Model. *Structures* **2024**, *63*, 106353. [CrossRef]
25. Miano, A.; Di Carlo, F.; Mele, A.; Giannetti, I.; Nappo, N.; Rompato, M.; Striano, P.; Bonano, M.; Bozzano, F.; Lanari, R.; et al. GIS Integration of DInSAR Measurements, Geological Investigation and Historical Surveys for the Structural Monitoring of Buildings and Infrastructures: An Application to the Valco San Paolo Urban Area of Rome. *Infrastructures* **2022**, *7*, 89. [CrossRef]
26. Sanabria, M.P.; Guardiola-Albert, C.; Tomás, R.; Herrera, G.; Prieto, A.; Sánchez, H.; Tessitore, S. Subsidence Activity Maps Derived from DInSAR Data: Orihuela Case Study. *Nat. Hazards Earth Syst. Sci.* **2014**, *14*, 1341–1360. [CrossRef]
27. Milillo, P.; Giardina, G.; DeJong, M.; Perissin, D.; Milillo, G. Multi-Temporal InSAR Structural Damage Assessment: The London Crossrail Case Study. *Remote Sens.* **2018**, *10*, 287. [CrossRef]
28. Cigna, F.; Tapete, D. Present-Day Land Subsidence Rates, Surface Faulting Hazard and Risk in Mexico City with 2014–2020 Sentinel-1 IW InSAR. *Remote Sens. Environ.* **2021**, *253*, 112161. [CrossRef]
29. Ezquerro, P.; Del Soldato, M.; Solari, L.; Tomás, R.; Raspini, F.; Ceccatelli, M.; Fernández-Merodo, J.A.; Casagli, N.; Herrera, G. Vulnerability Assessment of Buildings Due to Land Subsidence Using InSAR Data in the Ancient Historical City of Pistoia (Italy). *Sensors* **2020**, *20*, 2749. [CrossRef] [PubMed]
30. Shahbazi, S.; Barra, A.; Gao, Q.; Crosetto, M. Detection of Buildings with Potential Damage Using Differential Deformation Maps. *ISPRS J. Photogramm. Remote Sens.* **2024**, *218*, 57–69. [CrossRef]